Advances in Nano Research, *Vol. 12, No. 4 (2022) 415-426*
https://doi.org/10.12989/anr.2022.12.4.415

Visible light assisted photocatalytic degradation of methylene blue dye using Ni doped Co-Zn nanoferrites

Preeti Thakur*[1], Deepika Chahar[1] and Atul Thakur[2]

[1]*Department of Physics, Amity School of Applied Sciences, Amity University Haryana, 122413 India*
[2]*Centre for Nanotechnology, Amity University Haryana, 122413 India*

(*Received September 7, 2021, Revised January 27, 2022, Accepted January 28, 2022*)

Abstract. Nickel substituted cobalt-zinc ferrite nanoparticles with composition $Co_{0.5}Zn_{0.5}Ni_xFe_{2-x}O_4$ (x = 0.25, 0.5, 0.75, 1.0) were synthesized using a wet chemical method named citrate precursor method. Various characterizations of the prepared nanoferrites were done using X-ray powder diffractometry (XRD), Scanning electron microscopy (SEM), UV visible spectroscopy and Fourier transform spectroscopy technique (FT-IR). XRD confirmed the formation of cubic spinel structure of the samples with single phase having one characteristic peak at (311). The value of optical band gap (E_g) was found to decrease with Ni substitution and have values in the range 2.30eV to 1.69eV. A Fenton-type system was created by photocatalytic activity using source of visible light for removal of methylene blue dye. Observations revealed increase in the degradation of methylene blue dye with increasing nickel content in the samples. The degradation percentage was increased from 77.32% for x = 0.25 to 90.16% for x = 1.0 in one hour under the irradiation of visible light. Also, the degradation process was found to have pseudo first order kinetics model. Hence, it can be observed that synthesized nickel doped cobalt-zinc ferrites have good capability for water purification and its degradation efficiency enhanced with increase in nickel concentration.
Keywords: degradation; Fenton-type; photocatalytic mechanism; porosity; spinel

1. Introduction

Due to the efficient and versatile optical, magnetic, electrical and chemical properties of spinel ferrites, these materials are extensively studied by the researchers from past decades. These properties make these materials different from their bulk counterparts (Bhalla *et al*. 2021, Agrawal *et al*. 2016, Singh *et al*. 2015, Thakur *et al*. 2008). Spinel ferrites have a lot of applications in many fields like supercapacitors, magnetic sensors, MRI imaging, catalysis and as anti bacterial agents (Chahar *et al*. 2020, Samavati *et al*. 2017, Salazar-kuri *et al*. 2017, Kalpakli 2015, Xiong *et al*. 2014, Singh *et al*. 2014, Asghar *et al*. 2012, Yang *et al*. 2010, Mathur *et al*. 2008a, b). The spinel ferrites having general formula XFe_2O_4, (where X is any metal, for example Mg, Co, Ni, Zn, Mn) are being synthesized by the researchers from past some years. Magnetic ferrites like cobalt ferrite ($CoFe_2O_4$), manganese ferrite ($MnFe_2O_4$), zinc ferrite ($ZnFe_2O_4$), and copper ferrite ($CuFe_2O_4$) can be used as an efficient catalyst for the photocatalytic process. There are a lot of techniques for synthesizing spinel ferrite nanoparticles like sol-gel autocombustion, microwave combustion, co-precipitation and solvothermal etc. (Taneja *et al*. 2021, Thakur *et al*. 2018, Chen *et al*. 2017, Ma *et al*. 2017, Kurtinaitiene *et al*. 2016, Sharma *et al*. 2016, Theopil Anand *et al*. 2015, Atif *et al*. 2014, Mathur *et al*. 2010). Among all these methods citrate precursor method has a lot of advantages like lower time consumption, simple process, environmentally safe and low energy consumption. During recent years, there is tremendous rise in the environmental pollution because of the release of industrial wastewater which contains phenolic derivatives, synthetic pigments, and organic colouring contribution causing significant environmental hazards. These contaminants cause serious problems to aquatic life system due to their nondegradable nature. The effluents released from the textile and dye industries can be degraded using nanomaterials (Ikram *et al*. 2020, Raza *et al*. 2020, Girgis *et al*. 2015, Mondal *et al*. 2015). Many semiconducting materials like TiO_2, ZnO, and Sn_3O_4 etc. are being used as photocatalysts which behave as sensitizers for redox processes that are light-induced (Khademalrasool *et al*. 2020, Manzoor *et al*. 2018, Balgude *et al*. 2020). Spinel ferrites are considered efficient photocatalyst due to abundant availability, stability, non-toxic nature and simple process for the synthesis (Chahar *et al*. 2021, Chang *et al*. 2020, Balgude *et al*. 2020, Kapoor *et al*. 2018, Mahmoodi *et al*. 2014).

The life is affected due to increasing population, urbanization and industrialization. Water bodies are being excessively contaminated and causing severe threat to aquatic life forms and human beings. Organic dyes are released from printing, food, textile and leather industries (Bharagava 2018). These dyes are removed from water using various methods like adsorption (Ojemaye *et al*. 2019, Das *et al*. 2018), microbial degradation (Zhu *et al*. 2007), chemical precipitation (Sen *et al*. 2016) etc. These all processes are very costly, produce sludge and cause formation of secondary pollutants. Photocatalytic degradation using visible light can be opted as an efficient process for dye degradation.

Main cause of water pollution is the Methylene blue

*Corresponding author, Ph.D.,
E-mail: pthakur@ggn.amity.edu

ISSN: 2287-237X (Print), 2287-2388 (Online)

(MB), $C_{16}H_{18}N_3SCl$, an organic dye which is released from many textile and printing industries (Arora *et al*. 2019). Many health issues are caused due to this dye like nausea, vomiting, anemia, diarrhea and increase eutrophication (Jack Clifton *et al*. 2003) resulting in an imbalance of the aquatic ecosystem causing fatal effects to fauna and flora (Ekambaram *et al*. 2018). In the past times, methods used for treating industrial waste were chemical coagulation, biological, and adsorption methods but these methods are not efficient for the degradation of methylene blue dye from water completely. So, now a days, methods used for wastewater treatment are advanced oxidative processes (AOPs) (Ge *et al*. 2011). In this process, the .OH radicals are generated from oxidants like H_2O_2, O_3, and O_2. The improvement in efficiency of dye degradation can be done by doping of transition metal ions and using different light sources for the irradiation like UV light or visible light to increase the generation of .OH radicals.

Researchers are using spinel ferrite nanoparticles for the photocatalytic process due to their narrow band gap, high stability and magnetic nature. Organic pollutants are being removed by many researchers using spinel ferrite nanoparticles. Dhiman degraded remazol brilliant yellow and safranine-O using nickel ferrite prepared using hydrothermal route by visible light induced photocatalytic degradation (Dhiman *et al*. 2016). Also, methylene blue dye was degraded at pH 2.5 by Sharma using MFe_2O_4 (M= Ni, Co, Cu, Zn) in visible light and Fenton type system using H_2O_2 as a catalyst (Sharma *et al*. 2015).

The photo Fenton is really efficient for the dye degradation as it produces more oxidative hydroxyl radicals (.OH) that helps to stimulate the reaction (Kurian *et al*. 2015, Dutta *et al*. 2001). In this method, light sources, semiconductors and oxidants are used to decompose the organic pollutants. The organic pollutants are completely decomposed into non toxic Co_2 and H_2O. Cobalt ferrites were used by Abulkalam to degrade methylene blue dye using visible light radiations and H_2O_2 (Kalam *et al*. 2018). Also, by using nickel ferrite, the MB dye degradation reached upto 99% by photocatalytic degradation using H_2O_2 (Vinosha *et al*. 2018). The band gap of spinel ferrite nanoparticles lies in the visible region. Due to this reason, researchers have focused on the synthesis of nanoferrite particles and studied morphological and optical properties of these synthesized ferrites. The removal of methylene blue dye using photocatalytic mechanism was studied by Cao using CES- derived zinc ferrites (Cao *et al*. 2017). Cobalt ferrites were synthesized using hydrothermal method and degradation efficiency of the prepared ferrites for the removal of Reactive Red 4 dyes was checked (Habibi *et al*. 2015). Aluminium doped zinc ferrites were used by Borhan for the degradation of orange I dye (Borhan *et al*. 2014). Also, the removal of cationic triarylmethane dyes was processed by using cobalt ferrite nanoparticles (Sakti *et al*. 2020). Therefore, by introducing metal ion in the ferrite lattice, we can alter various properties of the nanoferrite particle. But the use of metal substituted cobalt zinc nanoferrite to degrade the methylene blue dye have been studied to a very limited extent. From the literature it has been found that the transition metals act as good catalyst, therefore we opted to investigate Ni doped Co-Zn nanoferrites as photocatalyst for the degradation of methylene blue dye. The present work investigates the degradation of methylene blue dye from the aqueous solutions by visible light induced photocatalytic activity using Ni doped Co-Zn nanoferrites with composition $Co_{0.5}Zn_{0.5}Ni_xFe_{2-x}O_4$ (x = 0.25, 0.5, 0.75 and 1.0) synthesized by citrate precursor method which is simple, easy to handle, economic and consumes less time.

2. Experimental work

2.1 Synthesis

Nickel doped cobalt – zinc nanoferrites are synthesized using citrate precursor technique. It is a wet chemical method in which citric acid plays the role of a chelating agent. Citric acid and metal nitrates are mixed to form a homogeneous solution. For the synthesis of ferrite nanoparticles, all the required metal nitrates that include zinc nitrate (98% purity), cobalt nitrate (99% purity), nickel nitrate (98% purity), and ferric nitrate (98% purity) were dissolved in distilled water in proper proportion along with citric acid to form a homogeneous solution. The mixture was kept for continuous stirring along with heating at a temperature of 80°C using a magnetic stirrer with a hot plate. After some hours of heating, a dry precursor was obtained and the whole moisture was lost from the sample due to heating and we got the ferrite nanoparticles. The sintering of obtained powder was done at a temperature of 800°C for 3 hours in a muffle furnace at a heating rate of 5°C/min to get the desired nickel doped cobalt – zinc nanoparticles.

2.2 Characterizations

For the structural study of Ni substituted Co-Zn nanoparticles with composition $Co_{0.5}Zn_{0.5}Ni_xFe_{2-x}O_4$ (x = 0.25, 0.5, 0.75 and 1.0), the samples were characterized by X-ray diffraction in a bruker X-ray diffractometer with CuKα radiation having wavelength λ=1.5405Å with angle scan of 2θ values with a step size of scanning rate 0.02 from 10° to 70°. Fourier transform infrared spectroscopy (FTIR) was analyzed on a Perkin Elmer FT-IR instrument in the range 4000 cm^{-1} to 400 cm^{-1}. The investigation of surface morphology of the synthesized samples was done using a Zeiss EVO40 scanning electron microscope (SEM). AXIS X-ray photoelectron spectrometer (UK) with Al K alpha monochromatic excited radiation was used for the analysis. The absorbance of methylene blue at fixed time intervals was checked by using UV visible spectroscopy. The Quantachrome instrument was used to calculate BET surface area from N_2 adsorption desorption isotherms.

2.3 Photocatalytic activity

The visible light induced photocatalytic degradation process on methylene blue dye was performed using the as-prepared Ni doped Co-Zn nanoferrite samples sintered at 800°C. For this process, 100 ml of 10 mg/L methylene blue solution was taken in a beaker. After that, 5 mg of the Ni

doped Co-Zn ferrite powder sample was mixed into it. Then, the prepared aqueous solution was put in dark for 45 minutes on a magnetic stirrer at room temperature so that adsorption desorption equilibrium can be attained between prepared dye solution and ferrite catalyst. After that, 0.1 ml of 30% H_2O_2 was dropwise added to the solution so that a Fenton type system can be created followed by exposing the solution to visible light using a light source of 300W tungsten lamp. The methylene blue dye samples were taken after regular time intervals (0 min, 20 min, 40 min and 60 min respectively) to check the degradation of dye from the aqueous solution. The absorbance of methylene blue dye from the solution was checked by UV visible spectroscopy.

3. Result and discussion

3.1 X-ray diffraction spectroscopy

XRD patterns of synthesized nickel doped Co-Zn nanoferrites prepared using citrate precursor method are shown by Fig. 1. The diffraction peaks that are indexed to lattice planes (220), (311), (222), (400), (422), (511), (440) at different 2θ values are shown by XRD patterns. All the observed peaks revealed the single phase spinel cubic structure having Fd-3m space group of the prepared ferrite samples. The characteristic peak detected at (311) showed the spinel phase whereas other peaks at (220), (222), (400), (422), (511) and (440) planes showed cubic structure of the synthesized ferrite nanoparticles (Rana *et al*. 2015, Sharma *et al*. 2016, Mathur *et al*. 2008a, b).

The average crystallite size values were calculated by using Scherer's equation:

$$D = \frac{K\,\lambda}{\beta \cos\theta} \tag{1}$$

where *D* is crystalline size, K is the shape factor which is dimensionless having typical value 0.89, λ is X-ray wavelength, β is full width at half maxima of the diffraction peaks and θ is diffraction angle. The values of average crystallite size were calculated in the range 37 nm to 41 nm for different concentrations of Ni ions.

The values of lattice parameter 'a' were calculated using equation:

$$a = d_{hkl}(h^2 + k^2 + l^2)^{1/2} \tag{2}$$

where d_{hkl} is interplanar spacing; h, k, l are miller indices and a is lattice parameter. There is regular increase in the value of the lattice parameter and the values are 8.40Å, 8.42Å, 8.44Å and 8.46Å for Ni^{2+} ions concentration x = 0.25, 0.50, 0.75 and 1.0 respectively. The increase in values of lattice parameter may be because of the large ionic radii of nickel ions (i.e. 0.72Å) in comparison with ferric ions (0.63Å).

The theoretical density was calculated using the below given equation:

$$\rho_{theoretical} = \frac{8M}{Na^3} \tag{3}$$

where, *N* is Avogadro number, *M* is molecular mass of the sample and *'a'* is the lattice parameter. A decreasing trend

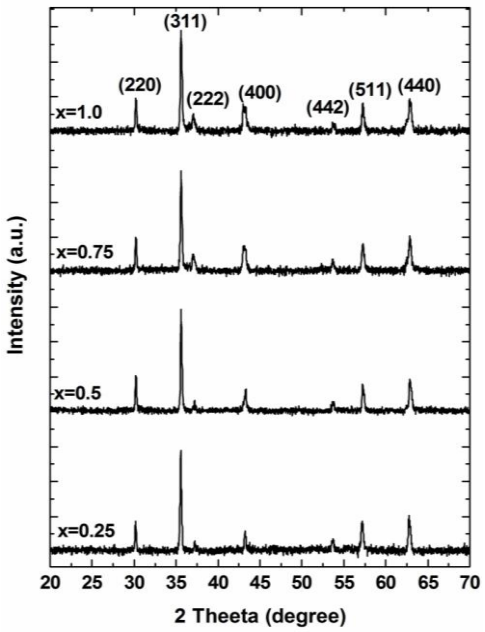

Fig. 1 X-ray diffraction patterns of Ni doped Co-Zn nanoferrites

Table 1 Various XRD parameters calculated using X-ray diffractometry

Concentration of nickel ions	Crystallite size (nm)	Theoretical density (g/cm^3)	Experimental density (g/cm^3)	Porosity (%)
0.25	40	5.33	8.25	53.18
0.5	41	5.32	7.99	50.15
0.75	37	5.26	7.42	41.04
1.0	38	5.25	7.11	35.25

was shown by the calculated theoretical density with increase in nickel concentration and its value lie in the range 5.33 g/cm^3 to 5.26 g/cm^3 for the prepared samples. The value of bulk density was calculated and it was found in the range 8.25 to 7.11 g/cm^3 and it showed a decreasing trend with increasing x value. The formula for calculation of bulk density is

$$d_{bulk} = \frac{mass}{volume} \tag{4}$$

The porosity percentage was calculated using following equation

$$Porosity\% = \left(1 - \frac{d_{exp.}}{d_{theoretical}}\right) \times 100 \tag{5}$$

The value of the porosity percentage decreased from 54.18% to 35.14% with increasing value of x. The porosity decreased due to increase in grain size with substitution of Ni^{2+} ions in place of Fe^{3+} ions. The calculated parameters are given in Table 1.

3.2 SEM/EDS analysis

To study the morphology and shape of the nanoferrite particles, the Scanning electron microscopy (SEM) analysis

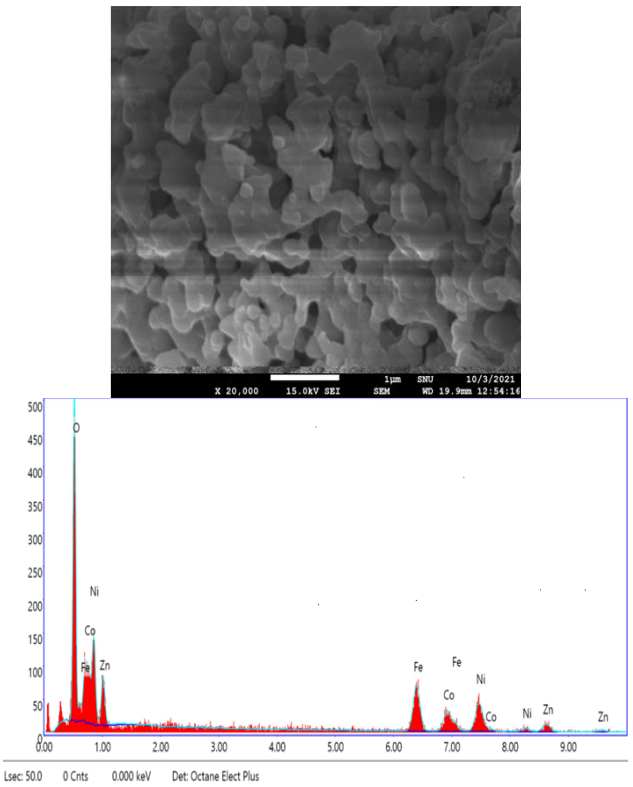

Fig. 2 SEM and EDS spectrum of $Co_{0.5}Zn_{0.5}Ni_xFe_{2-x}O_4$ for x = 1.0

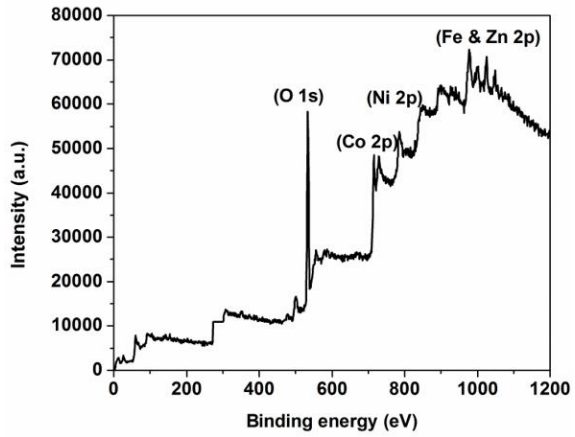

Fig. 3 XPS spectrum of synthesized Ni doped Co-Zn nanoferrites for x = 1.0

was done. Fig. 2 shows the SEM image and energy dispersive X-ray spectroscopy having elemental analysis of $Co_{0.5}Zn_{0.5}Ni_xFe_{2-x}O_4$ for x = 1.0.

Cubic sized grains having average grain diameter ~100 nm are shown by SEM images. The difference in average grain size is due to agglomeration and cluster formation by the synthesized ferrite nanoparticles. EDS spectrum confirms that there is no impurity and extra element in the synthesized nanoferrite sample.

3.3 X-ray photoelectron spectroscopy

Low resolution full scan XPS spectrum of Ni doped Co-Zn nanoferrites for x = 1.0 is shown in Fig. 3. The spectrum

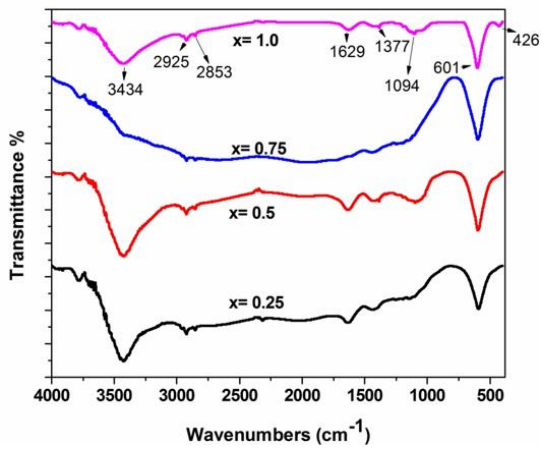

Fig. 4 FT-IR spectra of Ni doped Co-Zn ferrites for different concentrations of Ni ions

shows the peaks which correspond to the binding energies of Co 2p, Zn 2p, Ni 2p, Fe 2p and O 1s (Nesbitt *et al*. 2000, Vinuthna *et al*. 2013, Bera *et al*. 2001).The binding energies at around 1024 and 1046 eV are exhibited by the Zn, which are attributed to $Zn2p_{3/2}$ and $Zn2p_{1/2}$ electrons present in Zn^{2+} oxidation state respectively. The peaks around 714 eV and 727 eV are designated to $Fe2p_{3/2}$ and $Fe2p_{1/2}$ states. The presence of Fe^{3+} cations at octahedral site of the spinel structure is depicted by the peak at 714 eV and the peak at 727 eV reveals the Fe^{2+} cations present at tetrahedral sites. The major peaks with binding energy values at 793eV are attributed to the $Co2p_{1/2}$ states. The presence of Ni element was observed in the range 852-858 eV and 865-875 eV corresponding to Ni $2p_{3/2}$ and Ni $2p_{1/2}$ electrons present in the Ni^{2+} oxidation state respectively. The presence of oxygen was depicted by O1s spectrum in two different binding energy states in the range 531 eV to 542 eV.

3.4 FTIR Spectroscopy

Fig. 4 depicts the Fourier transform infrared spectra of the samples displaying chemical composition of the prepared ferrites via the modes of vibration for nickel doped cobalt – zinc ferrite nanoparticles.

The bands observed at 601 cm^{-1} and 426 cm^{-1} are attributed to the intrinsic stretching vibrations of metal ions at tetrahedral sites (A-sites) and octahedral sites (B-sites) (Coutinho *et al*. 2017). The CoOOH hydration of water is shown by the band present at 1094 cm^{-1}. The band appearing at 1377 cm^{-1} may be due to the moisture present in the system of FeOOH and nitrate ions (Habibi *et al*. 2014). Also, the bending modes of O-H bonds of absorbed water are present in the samples which are shown by the band around 1629 cm^{-1} (Suwanchawalit *et al*. 2015, Sivakumar *et al*. 2014). The C-H stretching vibrations are shown by the two characteristic bands observed at 2925 and 2853 cm^{-1}. A broad band around 3434 cm^{-1} is due to modes of O-H groups of water molecule.

3.5 Optical properties

UV visible spectroscopy measurements were done by using Diffused reflectance (DRS) to study the effect of Ni

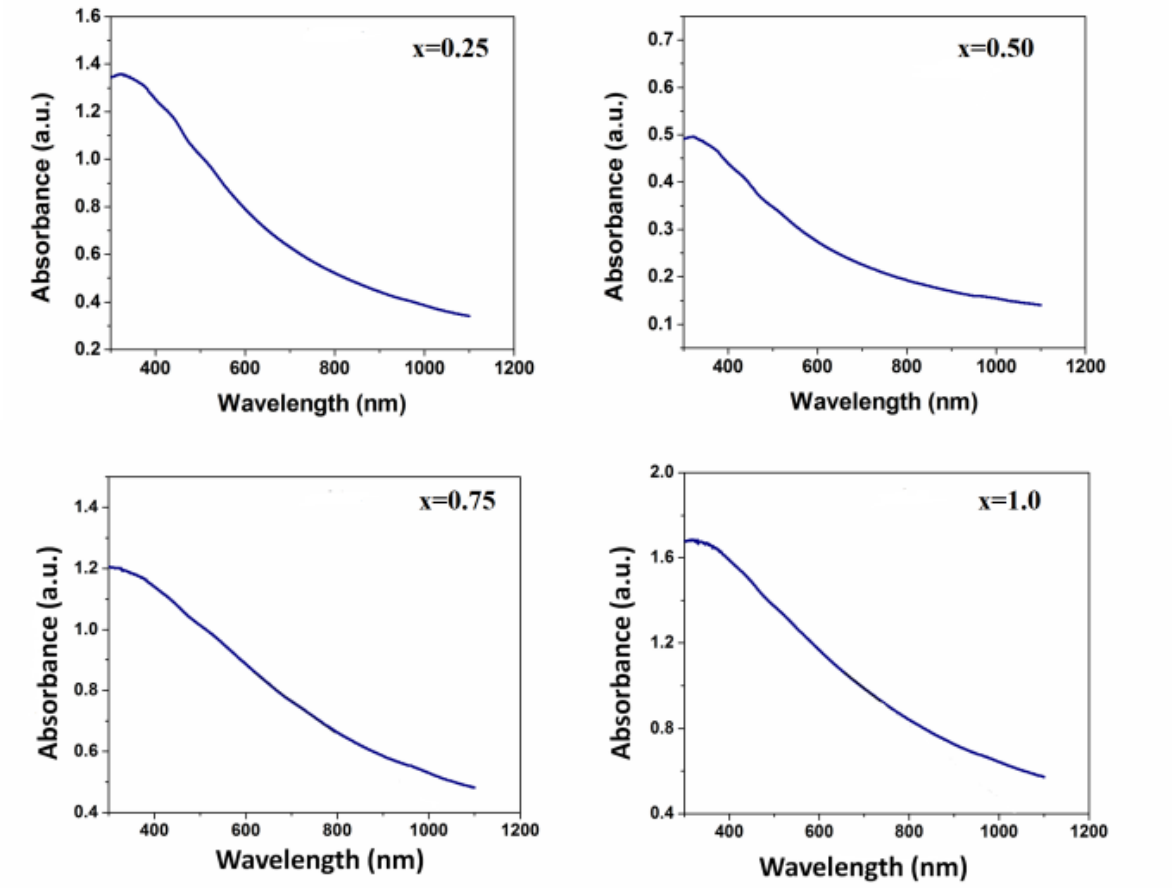

Fig. 5 Diffused UV-visible spectra of $Co_{0.5}Zn_{0.5}Ni_xFe_{2-x}O_4$ (x = 0.25, 0.50, 0.75 and 1.0) respectively

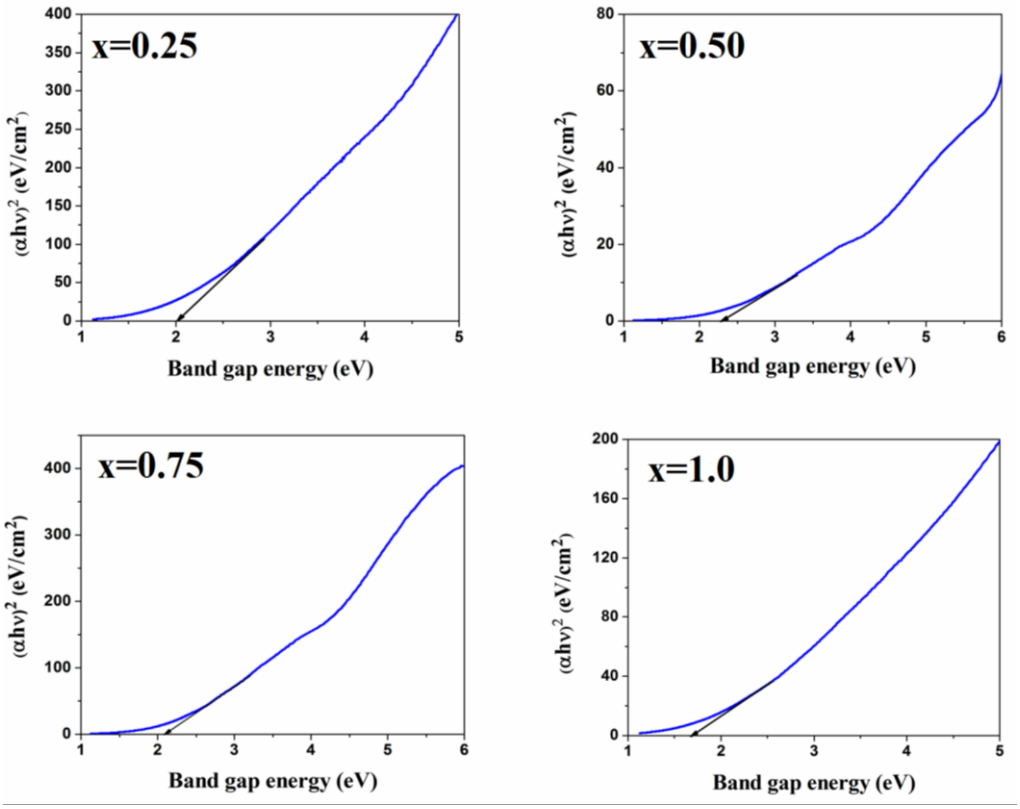

Fig. 6 Plots of $(\alpha h\nu)^2$ versus hν showing the band gap of $Co_{0.5}Zn_{0.5}Ni_xFe_{2-x}O_4$ (x = 0.25, 0.50, 0.75 and 1.0) respectively

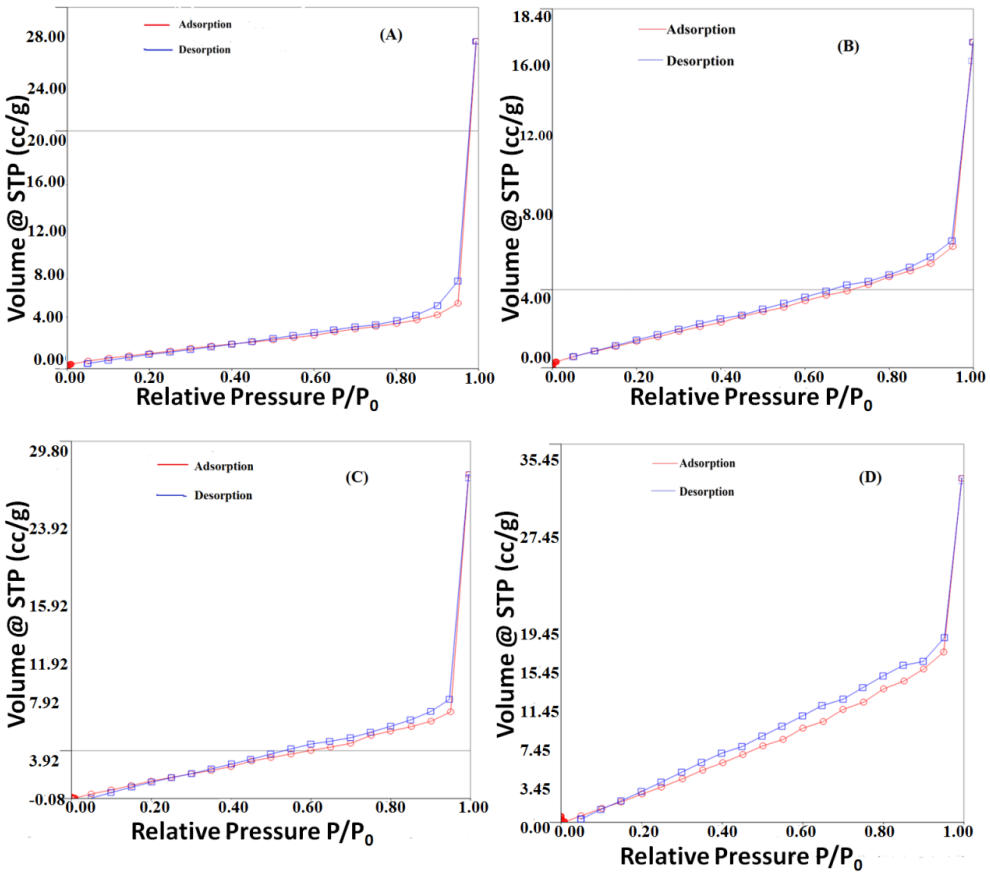

Fig. 7 (A-D) Nitrogen adsorption isotherms of synthesized $Co_{0.5}Zn_{0.5}Ni_xFe_{2-x}O_4$ (x = 0.25, 0.50, 0.75 and 1.00)

doping on $Co_{0.5}Zn_{0.5}Ni_xFe_{2-x}O_4$ nanoferrites. Fig. 5 shows the typical band edge absorption spectra of synthesized nanoferrites.

The absorbance was found to be significant for photocatalytic reactions with wavelength ranging from 800-1000 nm which covers the visible region. With increase in Ni doping, band edge absorption increased and values are found to be 904 nm, 984 nm, 1026 nm and 1036 nm for x = 0.25, 0.50, 0.75 and 1.0 respectively. The equation used to calculate the optical band gap (E_g) near the absorption edge is given as (Silambarasan *et al.* 2014)

$$\alpha h\nu = A(h\nu - E_g)^{1/2} \quad (6)$$

where, α is absorption coefficient, h is Planck's constant, ν is frequency of incident photon, A is proportionality constant and E_g is optical band gap. The graphs plotted between $(\alpha h\nu)^2$ and photon energy (hν) are shown in Fig 6.

The values of band gap were estimated from the graphs and found to have values 1.78eV, 2.30eV, 2.11eV and 1.69eV for Ni^{2+} ion concentration x = 0.25, 0.50, 0.75 and 1.0 respectively. The calculated values of optical band gap are given in Table 2. The optical band gap values firstly show an increase and then found to decrease with increase in Ni substitution in Co-Zn nanoferrite particles.

3.6 BET specific surface area study

The N_2 adsorption/desorption hysteresis loops of the synthesized Ni doped Co-Zn nanoferrites are shown in Fig. 7. All the isotherms of the ferrites exhibited type IV isotherms in accordance with IUPAC classification confirming the mesoporous nature of the prepared nanoferrite samples (Schneider *et al.* 1995). In mesoporous nature, the process of adsorption proceeds multilayer adsorption which is then followed by capillary condensation. The Ni doped samples were investigated for total surface area using N_2 adsorption/desorption isotherm.

The adsorbed gases and moisture were removed from the surface of the samples by degassing at 250°C for 3h. The equation given by Brunauer, Emmett and Teller was used to determine total BET surface area,

$$\frac{1}{Q\left[\left(\frac{P_0}{P}\right)-1\right]} = \frac{C-1}{Q_m C}\left(\frac{P}{P_0}\right) + \frac{1}{Q_m C} \quad (7)$$

here, P is the equilibrium pressure, P_0 is the saturation pressure, Q_m is the quantity of monolayer adsorbed gas, Q is the amount of N_2 gas adsorbed on the adsorbate and C is the BET constant.

The values of BET surface area of the prepared Ni doped Co-Zn samples were found to be $5.546 m^2/g$, $6.273 m^2/g$, $11.045 m^2/g$ and $75.742 m^2/g$ for Ni^{2+} ion concentration x = 0.25, 0.50, 0.75 and 1.00 respectively. The larger surface area means there is an increased number of active sites at surface for adsorption of reactive molecule resulting in more efficient photocatalytic process (Saroukhani *et al.* 2015). The calculated BET surface area increases with an increase in the Ni doping and the sample with Ni^{2+} ion concentration x = 1.00 has maximum surface area. The

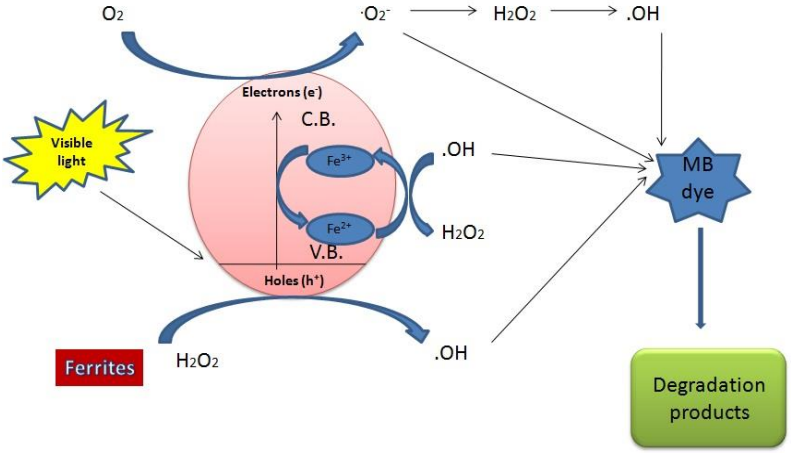

Fig. 8 Schematic diagram of photocatalytic degradation under visible light

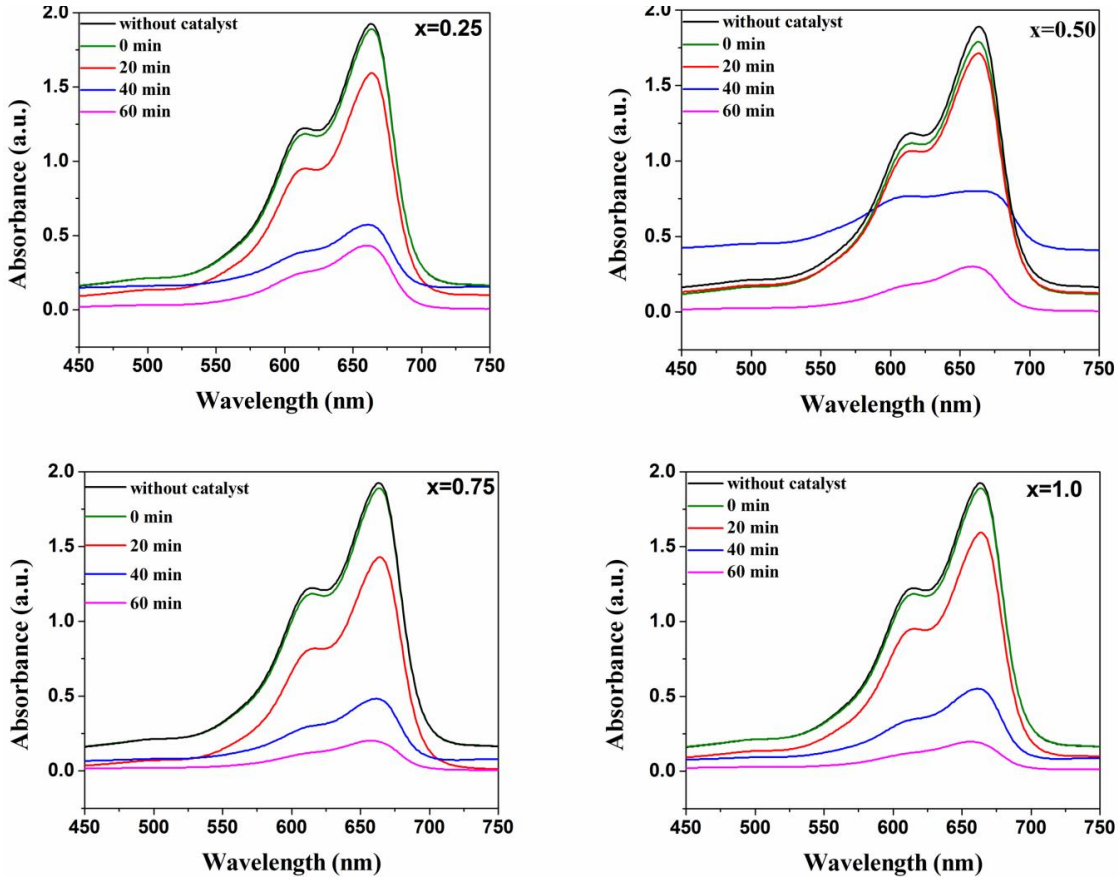

Fig. 9 UV visible spectra of methylene blue dye for different concentration of Ni ions

prepared nanoferrite samples were proved to be having good catalytic properties due to high surface area.

3.7 Photocatalytic study

3.7.1 Photocatalytic process

Nanophotocatalysis has proved to be very successful and efficient technique for the degradation of harmful organic substances from water at room temperature because these materials are chemically stable, less toxic, easily available and have very good photoactive properties due to their nano size (Yang 2021). Also, the photodegradation of organic pollutants is advantageous because this process is low cost, cause almost complete degradation and reusable. The use of magnetic photocatalysts is also preferred because the nanoparticles can be recovered using external magnetic fields and it allows numerous cycles of use of nanophotocatalysts. In actual, the process of photo-degradation of organic pollutants involves two steps: mineralization and degradation of pollutants (Umar *et al.* 2012). During the degradation process, the decomposition or splitting of organic pollutants into several products takes

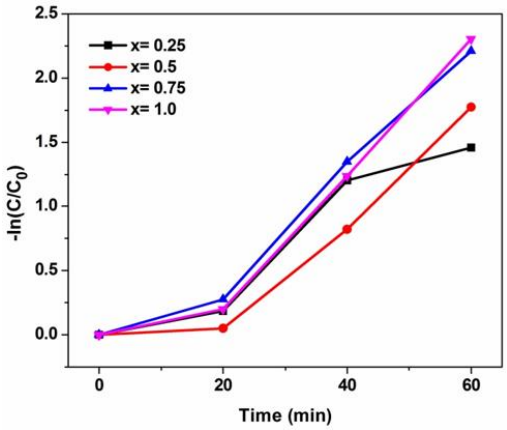

Fig. 10 Pseudo-first-order kinetics of methylene blue using $Co_{0.5}Zn_{0.5}Ni_xFe_{2-x}O_4$ (x=0.25, 0.5, 0.75 and 1.0) as a photocatalyst

Table 2 Effect of nickel ion concentration on the degradation of methylene blue

Concentration of nickel ions	Percentage degradation of dye in one hour	Rate constant 'k'	BET surface area (m^2/g)	Optical band gap (E_g) eV
0.25	77.32	0.0743	5.456	1.78
0.5	83.33	0.099	6.273	2.30
0.75	89.47	0.111	11.045	2.11
1.0	90.16	0.119	75.742	1.69

place. On the other hand, during mineralization, the organic pollutant is completely destructed into water, carbon dioxide and some inorganic ions. Some other oxidants like H_2O_2 are used with the photocatalysts during the photo-catalytic process so that a Fenton type system can be created by using ferrite catalysts under dark conditions or light irradiations (Guan *et al*. 2020, Wei *et al*. 2012, Sun *et al*. 2012).

In a Fenton type system, hydroxyl radicals are produced by the combination of ferrite nanophotocatalysts with H_2O_2 under light irradiation or dark conditions to enhance the degradation process. These generated .OH radicals (hydroxyl radicals) oxidize the organic contaminants present in wastewaters because of its potential (2.84 V versus the standard hydrogen electrode). The use of light enhances the degradation efficiency of the Fenton type system so that more organic pollutants can be degraded. The use of light in the process is responsible for the oxidation and reduction reactions. During the light irradiation, an electron (e^-) from the valence band get excited to the conduction band of the catalyst leaving a photogenerated hole (h^+) behind in the valence band. These produced electron and holes are responsible for the oxidation and reduction process. When photocatalytic mechanism takes place in aqueous solutions, water and hydroxide ions (OH^-reacts with photogenerated h^+ and form hydroxyl radicals (.OH), which act as primary oxidant in the oxidation of organic compounds during photocatalytic mechanism. The process of photocatalytic mechanism is shown by Fig. 8. The reactions showing the production of hydroxyl radicals in the photocatalytic mechanism are as under.

$$ferrites + hv \rightarrow e^- + h^+$$

$$O_2 + e^- \rightarrow O_2^{-\cdot}$$

$$OH^- + h^+ \rightarrow OH^{\cdot}$$

$$OH^{\cdot}/O_2^{-\cdot} + MB \rightarrow degraded\ products$$

3.7.2 Results of photocatalytic mechanism

Photocatalytic mechanism was used to degrade a dye named methylene blue from water by creating a photo Fenton type system using nickel doped cobalt zinc nano-ferrites. The prepared samples are proved to be very capable to degrade the methylene blue dye from water. UV visible spectra of methylene blue dye for different amount of Ni ions present in the samples is shown in Fig. 9. Two peaks appeared at 664 nm and 610 nm which validate the existence of methylene blue dye in the aqueous solution. The UV visible spectra of methylene blue show the concentration of dye present in water without adding catalyst and at different time intervals after irradiating with visible light. The degradation efficiency depends on the amount of doping, duration of contact time and generation of electron-hole pairs. As the content of Ni^{2+} ions was increased there is more degradation of methylene blue dye from water. The Fig. 9 shows regular decrease in the concentration of methylene blue dye in water as the contact time is increased. The concentration of methylene blue dye was calculated using the formula:

$$R\% = \frac{C_0 - C}{C} \times 100 \quad (8)$$

Here, C_0 is the initial concentration of the methylene blue at time t = 0 min and C is the final concentration of the methylene blue at time t = 1 hour after irradiating with visible light source.

The degradation of dyes using visible light irradiation is a pseudo first order kinetic model and its kinetics is demonstrated by using the equation (Vijay *et al*. 2019):

$$\ln\left(C/C_0\right) = -kt \quad (9)$$

Here, C_0 and C are the concentration of dye at time t = 0 and t respectively and k is equilibrium constant. The plots of -ln(C/C_0) versus irradiation time for all the Ni substituted Co-Zn samples are shown by Fig. 10. It can easily be seen from the figure that degradation of methylene blue using all the synthesized nanoferrite samples followed the pseudo first order kinetics.

The Fig. 11(a) shows that as the Ni^{2+} ion concentration was increased from x = 0.25 to x = 1.0, there was more removal of methylene blue dye from water. The degradation of dye was 77.32%, 83.33%, 89.47% and 90.16% for x = 0.25, 0.5, 0.75 and 1.0 respectively. The rate constant is computed using the relation:

$$k = 2.303 \times slope \quad (10)$$

Here, the 1st order kinetics graph is used to calculate slope. For x = 0.25, the value of rate constant is minimum i.e., 0.0743 but it increases as there is an increase in Ni content. It is 0.099, 0.1105 and 0.1198 for x = 0.5, 0.75 and

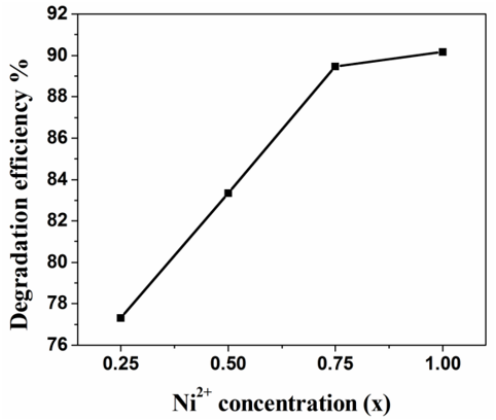

(a)

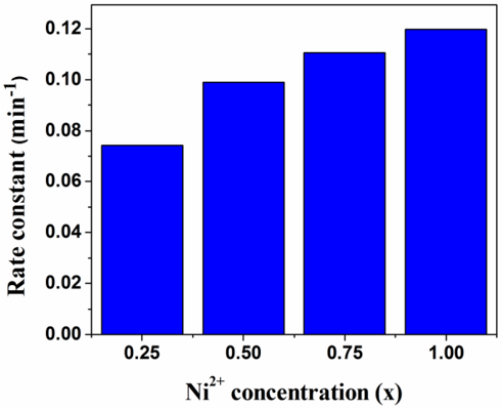

(b)

Fig. 11 (a) Degradation efficiency of methylene blue dye for different concentration of Ni^{2+} ions, (b) Plot of rate constant for photocatalytic activity of various samples

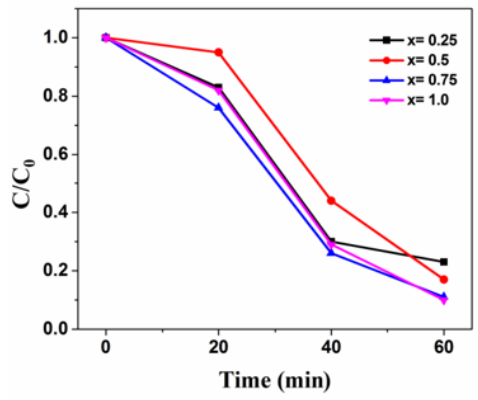

(a)

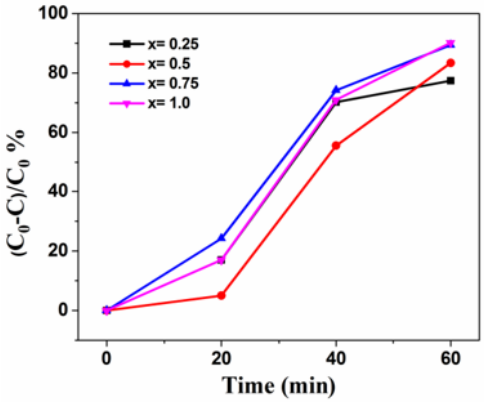

(b)

Fig. 12 (a) Photocatalytic degradation of methylene blue under visible light irradiation, (b) Time dependent percentage photodegradation of methylene blue for different nickel concentration

1.0 respectively. The dye degradation from water is a function of contact time.

The value of rate constant is found to rise with increase in the Ni ion concentration as shown in Fig. 11(b). The table 2 shows the values of rate constant calculated for different concentrations of Ni ions.

The Fig. 12(a) shows the contact time effect on the methylene blue degradation using visible light source by using 5 mg of the ferrite catalyst. Figure shows that with increase in time, the degradation of more methylene blue dye takes place. Also, the degradation increases with an increase in nickel doping in the Co-Zn ferrite lattice. The reason behind this may be that as the doping concentration is increased, more surface oxygen vacancies and defects are created that helps in promoting the photocatalytic degradation process. Low value of optical band gap may also increase the degradation of dye from water.

Fig. 12(b) shows the percentage degradation of methylene blue dye from water with time interval and it is observed that for all the Ni doped Co-Zn samples, the degradation of methylene blue dye get increased with time. The degradation of methylene blue after 1 hour was 77.32%, 83.33%, 89.47% and 90.16% for nickel concentration x = 0.25, 0.5, 0.75 and 1.0 respectively. A significant degradation is achieved in one hour for all the nickel doped Co-Zn samples and the degradation efficiency percentage increased with increase in time. Also, one more advantage of removal of methylene blue using photocatalytic activity is that, it is a safe process. In a Fenton type system, hydrogen peroxide is used which is safe, easy to handle and have no harmful effect on environment. The resultant products in this process are carbon dioxide and water.

4. Conclusions

The citrate precursor method was successfully used to synthesize nickel doped cobalt-zinc nanoferrite.

- XRD spectra of all the samples showed the single phase spinel cubic structure having characteristic peak at (311). The average crystallite size of the samples was in the range 37 nm to 41 nm.
- FT-IR spectroscopy confirmed the spinel crystal structure having stretching vibration of metal ions at tetrahedral and octahedral sites respectively.
- The optical band gap values found in the range 2.30 eV to 1.69 eV for Ni concentration varying from x = 0.25 to x = 1.0.
- The samples were found to have good BET surface area, to be used in adsorption processes.
- The degradation of methylene blue dye by nickel

substituted cobalt-zinc nanoferrites using photocatalytic mechanism was highlighted in present investigation. From the observations, it was noticed that there is increase in degradation efficiency with rise in nickel ion concentration from x = 0.25 to x = 1.0. The results revealed 90% removal of methylene blue from water in just 1 hour using synthesized ferrites.

• The degradation of the methylene blue dye was observed to be 77.32%, 83.33%, 89.47% and 90.16% for the nickel ion concentration x = 0.25, 0.5, 0.75 and 1.0 respectively. Also, pseudo-first-order kinetics model for removal of methylene blue was followed by all the substituted samples.

• The results showed that Ni doped Co-Zn nanoferrite particles act as powerful photocatalyst for removal of methylene blue dye from water without harming the environment.

References

Agrawal, S., Parveen A. and Azam A. (2016), "Structural, electrical, and optomagnetic tweaking of Zn doped $CoFe_{2-x}Zn_xO_4$ nanoparticles", *J. Magn. Magn. Mater.*, **414**, 114-152. https://doi.org/10.1016/j.jmmm.2016.04.059.

Arora, C., Soni, S., Sahu, S., Mittal, J., Kumar, P., Bajpai, P.K. (2019), "Iron based metal organic framework for efficient removal of methylene blue dye from industrial waste", *J. Mol. Liq.*, **284**, 343-352. https://doi.org/10.1016/j.molliq.2019.04.012.

Asghar, G., Rehman, M.A. (2012), "Structural, dielectric and magnetic properties of Cr-Zn doped strontium hexa-ferrites for high frequency applications", *J. Alloys Compd.*, **526**, 85-90. http://doi.org/10.1016/j.jallcom.2012.02.086.

Atif, M. and Nadeem, M. (2014), "Sol-gel synthesis of nanocrystalline $Zn_{1-x}Ni_xFe_2O_4$ ceramics and its structural, magnetic and dielectric properties", *J. Sol-Gel Sci. Technol.*, **72**(3), 615-626. https://doi.org/10.1007/s10971-014-3484-4.

Balgude, S., Barkade, S. and Mardikar, S. (2020), *Metal Oxides for High-Performance Hydrogen Generation by Water Splitting* in *Multifunctional Nanostructured Metal Oxides for Energy Harvesting and Storage Devices*, CRC press, Florida, U.S.A. https://doi.org/10.1201/9780429296871-6.

Balgude, S., Sethi, Y., Gaikwad, A., Kale, B., Amalnerkar, D. and Adhyapak, P. (2020), "Unique N doped Sn_3O_4 nanosheets as an efficient and stable photocatalyst for hydrogen generation under sunlight", *Nanoscale*, **12**(15), 8502-8510. https://doi.org/10.1039/C9NR10439A.

Bera, S., Prince, A.A.M., Velmurugan, S., Raghavan, P.S., Gopalan, R., Panneerselvam, G., Narasimhan, S.V. (2001), "Formation of zinc ferrite by solid state reaction and its characterization by XRD and XPS", *J. Mater. Sci.*, **36**(22), 5379-5384. https://doi.org/10.1023/A:1012488422484.

Bhalla, N., Taneja, S., Thakur, P., Sharma, P.K., Mariotti, D., Maddi, C., Ivanova, O., Petrov, D., Sukhachev, A., Edelman, I. S., Thakur, A. (2021), " Doping independent work function and stable band gap of spinel ferrites with tunable plasmonic and magnetic properties", *Nano Lett.*, **21**(22), 9780-9788. https://doi.org/10.1021/acs.nanolett.1c03767.

Bharagava, R.N. (2018), *Recent Advances in Environmental Management*, CRC Press, Florida, U.S.A.

Borhan, A.I., Samoila, P., Hulea, V., Iordan, A.R. and Palamaru, M.N. (2014), "Effect of Al^{3+} substituted zinc ferrite on photocatalytic degradation of Orange I azo dye", *J. Photochem. Photobiol., A*, **279**, 17-23. https://doi.org/10.1016/j.jphotochem.2014.01.010.

Cao, Z., Zhang, J., Zhou, J., Ruan, X., Chen, D., Liu, J., Liu, Q. and Qian, G. (2017), "Electroplating sludge derived zinc-ferrite catalyst for the efficient photo-Fenton degradation of dye", *J. Environ. Manage.*, **193**, 146-153. https://doi.org/10.1016/j.jenvman.2016.11.039.

Chahar, D., Taneja, S., Thakur, P., Thakur, A. (2020), "Remarkable resistivity and improved dielectric properties of Co-Zn nanoferrites for high frequency applications", *J. Alloys Compd.*, **843**, 15568. https://doi.org/10.1016/j.jallcom.2020.155681.

Chahar, D., Taneja, S., Bisht, S., Kesarwani, S., Thakur, P., Thakur, A., Sharma, P.B. (2021), "Photocatalytic activity of cobalt substituted zinc ferrite for the degradation of methylene blue dye under visible light irradiation", *J. Alloys Compd.*, **851**, 156878. https://doi.org/10.1016/j.jallcom.2020.156878.

Chang, F., Chen, Z., Jing, J. and Hou, J. (2020), "The photocatalytic phenol degradation mechanism of Ag-modifed ZnO nanorods", *J. Mater. Chem. C*, **8**(9), 3000-3009. https://doi.org/10.1039/C9TC05010H.

Coutinho, D.M., Verenkar, V.M.S. (2017), "Preparation, spectroscopic and thermal analysis of hexa- hydrazine nickel cobalt ferrous succinate precursor and study of solid-state properties of its nanosized thermal product", *J. Therm. Anal. Calorim.*, **128**(2), 807-817. https://doi.org/10.1007/s10973-016-6011-8.

Chen, W., Liu, D., Wu, W., Zhanga, H. and Wua, J. (2017), "Structure and magnetic properties evolution of rod-like $Co_{0.5}Ni_{0.25}Zn_{0.25}Dy_xFe_{2-x}O_4$ synthesized by solvothermal method", *J. Magn. Magn. Mater.*, **422**, 49-56. https//doi.org/10.1016/j.jmmm.2016.08.067.

Das, S., Dash, S.K., Parida, K.M. (2018), "Kinetics, isotherm and thermodynamic study for ultrafast adsorption of azo dye by an efficient sorbent: Ternary Mg/(Al+Fe) layered double hydroxides", *ACS Omega*, **3**(3), 2532-2545. https://doi.org/10.1021/acsomega.7b01807.

Dhiman, M., Goyal, A., Kumar, V., Singhal, S. (2016), "Designing different morphologies of $NiFe_2O_4$ for tuning of structural, optical and magnetic properties for catalytic advancements", *New J. Chem.*, **40**(12), 10418-10431. https://doi.org/10.1039/C6NJ03209E.

Dutta, K., Mukhopadhyaya, S., Bhattacharjee, S. and Chaudhuri, B. (2001), "Chemical oxidation of methylene blue using a Fenton-like reaction", *J. Hazard. Mater.*, **84**(1), 57-71. https://doi.org/10.1016/s0304-3894(01)00202-3.

Ekambaram, S.P., Perumal, S.S., Rajendran, D., Samivel, D., Khan, M.N. (2018), *New Approach of Dye Removal in Textile Effluent: A Cost-Effective Management for Cleanup of Toxic Dyes in Textile Effluent by Water Hyacinth* In *Toxicity and Biodegradation Testing*, Humana Press, New York, U.S.A. https://doi.org/10.1007/978-1-4939-7425-2_12.

Ge, L., Liu, J. (2011), "Efficient visible light-induced photocatalytic degradation of methyl orange by QDs sensitized CdS-Bi_2WO_6", *Appl. Catal. B Environ.*, **105**(3-4), 289-297. https://doi.org/10.1016/j.apcatb.2011.04.016.

Girgis, E., Adel, D., Tharwat, C., Attallah, O. and Rao, K.V. (2015), "Cobalt ferrite nanotubes and porous nanorods for dye removal", *Adv. Nano Res.*, **3**(2), 111-121. https://doi.org/10.12989/anr.2015.3.2.111.

Habibi, M.H. and Parhizkar, J. (2015), "Cobalt ferrite nano-composite coated on glass by Doctor Blade method for photo-catalytic degradation of an azo textile dye Reactive Red 4: XRD, FESEM and DRS investigations", *Spectrochim. Acta A*, **150**, 879-885. https://doi.org/10.1016/j.saa.2015.06.040.

Habibi, M.H., Parhizkar, H.J. (2014), "FTIR and UV-vis diffuse reflectance spectroscopy studies of the wet chemical (WC) route synthesized nano-structure $CoFe_2O_4$ from $CoCl_2$ and $FeCl_3$", *Spectrochim. Acta A*, **127**, 102-106. https://doi.org/10.1016/j.saa.2014.02.090.

Guan, S., Li, R., Sun, X., Xian, T., Yang, H. (2020), " Construction of novel ternary Au/$LaFeO_3$/Cu_2O composite photocatalysts for RhB degrdation via photo-Fenton catalysis", *Mater. Tech*., **36**(10), 603-615. https://doi.org/10.1080/10667857.2020,1782062.

Ikram, M., Khan, M.I., Raza, A., Imran, M., Ul-Hamid, A. and Ali, S. (2020), "Outstanding performance of silver-decorated MoS_2 nano petals used as nano catalyst for synthetic dye", *Physica E*, **124**, 114246. https://doi.org/10.1016/j.physe.2020.114246.

Jack Clifton, I.I., Leikin, J.B. (2003), "Methylene blue", *Am. J. Therapeut*., **10**(4), 289-291. https://doi.org/10.1097/00045391-200307000-00009.

Kalam, A., Al-Sehemi, A.G., Assiri, M., Du, G., Ahmad, T., Ahmad, I., Pannipara, M. (2018), "Modified solvothermal synthesis of cobalt ferrite ($CoFe_2O_4$) magnetic nanoparticles photocatalysts for degradation of methylene blue with H_2O_2/ visible light", *Results Phys*., **8**, 1046-1053. https://doi.org/10.1016/j.rinp.2018.01.045.

Kalpakli, Y. (2015), "Removal of Cu(II) from aqueous solutions using magnetite: A kinetic, equilibrium study", *Adv. Environ. Res.*, **4**(2), 119-133. https://doi.org/10.12989/aer.2015.4.2.119.

Kapoor, S., Goyal, A., Bansal, S. and Singhal, S. (2018), "Emergence of bismuth substituted cobalt ferrite nanostructures as versatile candidates for the enhanced oxidative degradation of hazardous organic dyes", *New J. Chem*., **42**(18), 14965-14977. https://doi.org/10.1039/C8NJ00977E.

Khademalrasool, M., Talebzadeh, M.D. and Farbod, M. (2020), "ZnO/Silver nanocubes nanocomposites: Preparation, characterization, and scrutiny of plasmon-induced photocatalysis activity", *J. Photochem. Photobiol., A*, **396**, 112561. https://doi.org/10.1016/j.jphotochem.2020.112561.

Kurian, M., Nair, D.S. (2015), "Heterogeneous Fenton behavior of nano nickel zinc ferrite catalysts in the degradation of 4-chlorophenol from water under neutral conditions", *J. Water Proc. Eng*., **8**, e37-e49. https://doi.org/10.1016/j.jwpe.2014.10.011.

Kurtinaitiene, M., Mazeika, K., Ramanavicius, S., Pakstas, V. and Jagminas, A. (2016), "Effect of additives on the hydrothermal synthesis of manganese ferrite nanoparticles", *Adv. Nano Res*., **4**(1), 1-14. https://doi.org/10.12989/anr.2016.4.1.001.

Ma, J., Chen, B., Chen, B., Zhang, S. (2017), "Preparation of superparamagnetic $ZnFe_2O_4$ submicrospheres via a solvothermal method", *Adv. Nano Res*., **5**(2), 171-178, https://doi.org/10.12989/anr.2017.5.2.171.

Mahmoodi, N.M., Abdi, J. and Bastani, D. (2014), "Direct dyes removal using modified magnetic ferrite nanoparticles", *J. Environ. Health Sci. Eng*., **12**(1), 96. https://doi.org/10.1186/2052-336X-12-96.

Manzoor, M., Rafiq, A., Ikram, M. (2018), "Structural, optical, and magnetic study of Ni-doped TiO_2 nanoparticles synthesized by sol-gel method", *Int. Nano Lett*., **8**(1), 1-8. https://doi.org/10.1007/s40089-018-0225-7.

Mathur, P., Thakur, A., Singh, M. (2008a), "Low temperature synthesis of $Mn_{0.4}Zn_{0.6}In_{0.5}Al_{0.1}Fe_{1.4}O_4$ nano-ferrite and characterization for high frequency applications", *Eur. Phys. J. Appl. Phys*., **41**(2), 133-138. https://doi.org/10.1051/epjap.2008003.

Mathur, P., Thakur, A., Singh, M., Harris, G. (2008b), "Preparation and Characterization of $Mn_{0.4}Ni_xZn_{0.6-x}Fe_2O_4$ soft spinel ferrites for low and High Frequency Applications by Citrate Precursor Method", *Zeitchrift fur Physikalische Chemie*, **222**(4), 621-633. https://doi.org/10.1524/zpch.2008.5265.

Mathur, P., Thakur, A., Lee, J.H., Singh, M.(2010), "Sustained electromagnetic properties of Ni-Zn-Co nanoferrites for the high-frequency applications", *Mater. Lett*., **64**(24), 2738-2741. https//doi.org/10.1016/j.matlet.2010.08.056.

Mondal, A., Mondal, A. and Mukherjee, D. (2015), "Room-temperature synthesis of cobalt nanoparticles and their use as catalysts for Methylene blue and Rhodamine-B dye degradation", *Adv. Nano Res*., **3**(2), 67-79. https://doi.org/10.12989/anr.2015.3.2.067.

Nesbitt, H.W., Legrand, D., Bancroft, G.M. (2000), "Interpretation of Ni2p XPS spectra of Ni conductors and Ni insulators", *Phys. Chem. Miner*., **27**(5), 357-366. https://doi.org/10.1007/s002690050265.

Ojemaye, M.O., Okoh, A.I. (2019), "Multiple nitrogen functionalized magnetic nanoparticles as an efficient adsorbent: synthesis, kinetics, isotherm and thermodynamic studies for the removal of rhodamine B from aqueous solution", *Sci. Rep*., **9**(1), 9672. https://doi.org/10.1038/s41598-019-45293-x.

Rana, K., Thakur, P., Sharma, P., Tomar, M., Gupta, V., Thakur, A. (2015), "Improved structural and magnetic properties of cobalt nanoferrites : Influence of sintering temperature", *Ceram. Int*., **41**(3), 4492-4497. https://doi.org/10.1016/j.ceramint.2014.11.143.

Raza, A., Qumar, U., Hassan, J., Ikram, M., Ul-Hamid, A., Haider, J., Imran, M. and Ali, S. (2020), "A comparative study of dirac 2D materials, TMDCs and 2D insulators with regard to their structures and photocatalytic/sono photocatalytic behavior", *Appl. Nanosci*., **10**(10), 3875-3899. https://doi.org/10.1007/s13204-020-01475-y.

Sakti, S.C.W., Laily, R.N., Aliyah, S., Indrasari, N., Fahmi, M.Z., Lee, H.V., Akemotod, Y. and Tanaka, S. (2020), "Recollectable and recyclable epichlorohydrin-cross linked humic acid with spinel cobalt ferrite core for simple magnetic removal of cationic triarylmethane dyes in polluted water", *J. Environ. Chem. Eng*., **8**(4), 104004. https://doi.org/10.1016/j.jece.2020.104004.

Salazar-Kuri, U., Estevez, J.O., Silva-Gonz´alez, N.R., Pal, Y. and Mendoza, M.E. (2017), "Structure and magnetic properties of the $Co_{1-x}Ni_xFe_2O_4$-$BaTiO_3$ core-shell nanoparticles", *J. Magn. Magn. Mater*., **442**, 247-254. https://doi.org/10.1016/j.jmmm.2017.06.126.

Samavati, A. and Ismail, A.F. (2017), "Antibacterial properties of copper-substituted cobalt ferrite nanoparticles synthesized by co-precipitation method", *Particuology*, **30**, 158-163. https://doi.org/10.1016/j.partic.2016.06.003.

Saroukhani, Z., Tahmasebi, N., Mahdavi, S.M., Nematip, A. (2015), "Effect of working pressure and annealing temperature on microstructure and surface chemical composition of barium strontium titanate films grown by pulsed laser deposition", *Bull. Mater. Sci*., **38**(6), 1645-1650. https://doi.org/10.1007/s12034-015-0982-0.

Scheider, P. (1995), "Review adsorption isotherms of microporous-mesoporous solids revisited", *Appl. Catal A-Gen*., **129**(2), 157-165. https://doi.org/10.1016/0926-860X(95)00110-7.

Sen, S.K., Raut, S., Bandyopadhyay, P. and Raut, S. (2016), "Fungal decolouration and degradation of azo dyes: A review", *Fungal Biol. Rev*., **30**(3), 112-133. https://doi.org/10.1016/j.fbr.2016.06.003.

Sharma, P., Thakur, P., Mattei, J.L., Queffelec, P., Thakur, A. (2016), "Synthesis, structural, optical, electrical and Mössbauer spectroscopic studies of Co substituted $Li_{0.5}Fe_{2.5}O_4$", *J. Magn. Magn. Mater*., **407**, 17-23. https://doi.org/10.1016/j.jmmm.2016.01.023.

Sharma, R., Bansal, S. and Singhal, S. (2015), "Tailoring the photo Fenton activity of spinel ferrites (MFe_2O_4) by incorporating different cations (M= Cu, Zn, Ni and Co) in the structure", *RSC Adv.*, **5**(8), 6006-6018. https://doi.org/10.1039/C4RA13692F.

Sharma, R., Thakur, P., Kuma, M., Thakur, N., Negi, N.S., Sharma, P. and Sharma, V. (2016), "Improvement in magnetic behaviour of cobalt doped magnesium zinc nano-ferrites via co-precipitation route", *J. Alloys Compd*., **684**, 569-581. https//doi.org/10.1016/j.jallcom.2016.05.200.

Silambarasan, A., Rajesh, P., Ramasamy, P. (2014), "Synthesis, growth, structural, optical and thermal properties of an organic

single crystal:4-Nitroaniline 4-aminobenzoic acid", *Spectrochim. Acta A*, **118**, 24-27. https//doi.org/10.1016/j.saa.2013.08.052.

Singh, C., Goyal, A. and Singhal, S. (2014), "Nickel-doped cobalt ferrite nanoparticles: Efficient catalysts for the reduction of nitro aromatic compounds and photo-oxidative degradation of toxic dyes", *Nanoscale*, **6**(14), 7959-7970. https://doi.org/10.1039/C4NR01730G.

Singh, C., Jauhar, S., Kumar, V., Singh, J. and Singhal, S. (2015), "Synthesis of zinc substituted cobalt ferrites via reverse micelle technique involving in situ template formation: A study on their structural, magnetic, optical and catalytic properties", *Mater. Chem. Phys.*, **156**, 188-197. https://doi.org/10.1016/j.matchemphys.2015.02.046.

Sivakumar, S., Anusuya, D., Khatiwada, C.P., Sivasubramanian, J., Venkatesan, A. and Soundhirarajan, P. (2014), "Characterizations of diverse mole of pure and Ni-doped a -Fe_2O_3 synthesized nanoparticles through chemical precipitation route", *Spectrochim. Acta A*, **128**, 69-75. https://doi.org/10.1016/j.saa.2014.02.136 .

Suwanchawalit, C. and Somjit, V. (2015), "Hydrothermal synthesis of magnetic $CoFe_2O_4$ -graphene nanocomposite with enhanced photocatalytic performance", *Digest J. Nanomater. Biostruct.*, **10**, 769-777.

Sun, S., Yang, X., Zhang, Y., Zhang, F. and Ding, J. (2013), "Enhanced photocatalytic activity of sponge-like $ZnFe_2O_4$ synthesized by solution combustion method", *Prog. Nat. Sci.*, **22**(6), 639-643. https://doi.org/10.1016/j.pnsc.2012.11.008.

Taneja S., Chahar, D., Thakur, P. and Thakur, A. (2021), "Influence of bismuth doping on structural, electrical and dielectric properties of Ni-Zn nanoferrites", *J. Alloys Compd.*, **859**, 157760. https://doi.org/10.1016/j.jallcom.2020.157760.

Thakur, A. and Singh, M.(2008), "Low temperature synthesis of $Mn_{0.4}Zn_{0.6}In_{0.5}Fe_{1.5}O_4$ nanoferrite for high-frequency applications", *J. Phys. Chem. Solids*, **69**(1), 187-192. https://doi.org/10.1016/j.jpcs.2007.08.014.

Thakur, P., Sharma, P., Luc, J., Patrick, M., Alex, Q., Sergei, V.T., Panina, L.V. and Thakur, A. (2018), "Influence of cobalt substitution on structural, optical, electrical and magnetic properties of nanosized lithium ferrite", *J. Mater. Sci.*, **29**(9), 16507-16515. https://doi.org/10.1007/s10854-018-9744-2.

Theopil Anand, G., Kennedy, L.J., Vijaya, J.J., Kaviyarasan, K. and Sukumar, M. (2015), "Structural, optical and magnetic characterization of $Zn_{1-x}Ni_xAl_2O_4$ ($0 <= x <= 0.5$) spinel nanostructures synthesized by microwave combustion technique", *Ceram. Int.*, **41**(1), 603-615. https//doi.org/10.1016/j.ceramint.2014.08.109.

Umar, K., Dar, A.A., Haque, M.M., Mir, N.A. and Muneer, M. (2012), "Photocatalysed decolourization of two textile dye derivatives, Martius Yellow and Acis Blue 129 in UV-irradiated aqueous suspensions of Titania", *Desal. Water Treat.*, **46**(1-3), 205-214. https://doi.org/10/1080/19443994.2012.677527.

Vijay, S., Balakrishnan, R.M., Rene, E.R. and Priyanka, U. (2019), "Photocatalytic degradation of Irgalite violet dye using nickel ferrite nanoparticles", *J. Water Supply Res. T.*, **68**(8), 666-674. https://doi.org/10.2166/aqua.2019.039.

Vinosha, P.A., Xavier, B., Anceila, D. and Das S.J. (2018), "Nanocrystalline ferrite (MFe_2O_4, M= Ni, Cu, Mn and Sr) photocatalysts synthesized by homogeneous co-precipitation technique", *Optik*, **157**, 441-448. https://doi.org/10.1016/j.ijleo.2017.11.016.

Vinuthna, C., Ravinder, D. and Raju, R.M. (2013), "Characterization of $Co_{1-x}Zn_xFe_2O_4$ nano spinel ferrites prepared by citrate precursor method", *Mater. Sci.*, **3**, 654-660. https://doi.org/10.1134/S1070427218080050.

Xiong, P., Hu, C., Fan, Y., Zhang, W., Zhu, J. and Wang, X. (2014), "Ternary manganese ferrite/graphene/polyaniline nanostructure with enhanced electrochemical capacitance performance", *J. Power Sources*, **266**, 384-392. https://doi.org/10.1016/j.jpowsour.2014.05.048.

Yang, H. (2021), "A short review on heterojunction photocatalysts: Carrier transfer behavior and photocatalytic mechanims", *Mater. Res. Bull.*, **142**, 111406. https://doi.org/10.1016/j.materresbull.2021.111406.

Yang, H., Zhang, C., Shi, X., Hu, H., Du, X., Fang, Y., Ma, Y., Wu, H. and Yang, S. (2010), "Water soluble superparamagnetic manganese ferrite nanoparticles for magnetic resonance imaging", *Biomaterials*, **31**(13), 3667-3673. https://doi.org/10.1016/j.biomaterials.2010.01.055.

Zhu, M.X., Lu, L., Wang, H.H. and Wang, Z. (2007), "Removal of an anionic dye by adsorption/precipitation processes using alkaline white mud", *J. Hazard Mater.*, **149**(3), 735-741. https://doi.org/10.1016/j.jhazmat.2007.04.037.

JL